KSCE Journal of Civil Engineering (2023) 27(11):4993-5007
DOI 10.1007/s12205-023-0889-z

pISSN 1226-7988, eISSN 1976-3808
www.springer.com/12205

Tunnel Engineering

Analytical Solution for Interaction between Tunnel Surrounding Rock and Supports in Red Sandstone Stratum

Zhen Li[a], **Haiyan Xu**[b], **and Zhijie Wang**[c]

[a]*Dept. of Geotechnical Engineering, College of Civil Engineering, Tongji University, Shanghai 200092, China*
[b]*School of Civil Engineering, Sichuan Agricultural University, Chengdu 611830, China*
[c]*Key Laboratory of Transportation Tunnel Engineering of Ministry of Education, Southwest Jiaotong University, Chengdu 610031, China*

ARTICLE HISTORY

Received 29 April 2023
Revised 3 July 2023
Accepted 21 July 2023
Published Online 16 September 2023

KEYWORDS

Circular tunnel
Red sandstone stratum
Analytical solution
Staged installation
Support flexibility

ABSTRACT

Improving the flexibility of the support system is an effective measure to prevent structural failure caused by large deformation of the surrounding rock in tunnels passing through red sandstone stratum. By utilizing the staged support installation method, the initial install location of the supports can be adjusted to control the flexibility of the support system. However, there is currently no corresponding analytical solution available to accurately predict the mechanical behavior of the surrounding rock and supports. This paper proposes an analytical solution for the whole process of interaction between the surrounding rock and supports. Firstly, based on the improved unified strength criterion and non-associated flow rule, an elastoplastic analysis of the surrounding rock of a circular tunnel in red sandstone stratum is conducted, which takes into account intermediate principal stress, dilatancy, and nonlinear strain-softening properties. Next, six types of interaction between the surrounding rock and supports are proposed, along with corresponding judge theorems. Furthermore, an analytical solution for the mechanical response of the surrounding rock and supports during the whole construction process are presented. After verifying its effectiveness, a parametric analysis is performed to investigate the influence of design parameters on the supporting effect. Finally, the application effect of the staged support installation method is compared with that of the traditional method, and the cost savings advantage of the former is demonstrated.

1. Introduction

Haoji Railway plays a critical role in China's comprehensive transportation system, crossing a range of challenging geological environments along its route. The red sandstone stratum is the most commonly encountered geological formation, characterized by dilatancy and strain-softening properties, making it susceptible to construction disturbance and exhibiting poor self-stability (Wang et al., 2021; Xu et al., 2021; Li et al., 2023). Construction of tunnels within the red sandstone stratum can result in substantial deformation of the surrounding rock. Implementing stiff supports that follow the resistance principle may lead to the crushing failure of the support structures due to overload. As an example, during the construction of Yangcheng Tunnel on the Haoji Railway, shotcrete cracking and steel frame distortion occurred, leading to damaged supports requiring reinstallation and significantly delaying construction efficiency (Wang et al., 2018). Enhancing support flexibility to optimize the utilization of self-bearing capacity in surrounding rock can prevent structural failure caused by large deformations (Zhao et al., 2022), achieving optimal balance between structural safety and deformation control.

Traditionally, stiffness-based support systems have struggled to cope with large deformations of the surrounding rock. To address this issue, the "resistance principle" has been supplanted by the "flexible method" (Wu et al., 2022a), which involves moderately releasing rock deformation to mitigate the pressure on support structures. Though the use of scalable support can hike up project costs, staged installation methods have been proposed as a method of improving support flexibility. In this approach, each component of the primary support system (e.g., steel frame, shotcrete) is installed at varying distances from the tunnel face, so the flexibility of the support system can be adjusted by changing

CORRESPONDENCE Haiyan Xu haiyanXU@my.swjtu.edu.cn School of Civil Engineering Sichuan Agricultural University, Chengdu 611830, China

the initial install location. Despite the promise of this method, there is still a need for theoretical methods that analyze the interaction between the surrounding rock and supports of the tunnel in the red sandstone stratum.

The interaction between the surrounding rock and support is rooted in three curves: the Ground Reaction Curve (GRC), Support Reaction Curve (SRC), and Longitudinal Deformation Profile (LDP) (Chu et al., 2019; Sun et al., 2021; Lin et al., 2023). According to the traditional convergence-confinement method, the intersection of the GRC and SRC represents the equilibrium state of the surrounding rock and support. It fails to take into account the spatial effects of the tunnel face, which makes it challenging to reflect the dynamic interactions between the surrounding rock and support accurately. To address this issue, some scholars have proposed coupling approaches that integrates the GRC, SRC, and LDP. For instance, Liu et al. (2023) proposed an analytical model to solve the time-dependent interaction between support structures and rheological rock, which takes the shotcrete progressive hardening property, tunnel excavation effect, and sequential installation of linings into account. Qiu et al. (2022) presented a simplified analytical method that considers the effects of tunnel excavation rate and tunnel face stress release in rheological rock, enabling the investigation of the tunnel face effect and rock mass time-dependent behavior. Zhou et al. (2021) decomposed the total support force into the virtual support force and artificial support structures, conducting a systemic parametric analysis on radial deformation of the tunnel and support force.

Through a review of the literature, it became evident that there is currently no established analytical solution for staged support installation. This deficiency makes it challenging to predict the mechanical response of the support system quickly or determine reasonable installation timing and stiffness for each supporting component. Moreover, the surrounding rock in the red sandstone stratum has multiple elastoplastic states due to dilatancy and softening characteristics, which can increase the complexity of the interaction mechanism between the surrounding rock and support system. As China's transportation infrastructure continues to develop rapidly, an increasing number of tunnel projects crossing stratum with engineering properties similar to those of the red sandstone stratum will emerge. The theoretical research detailed above is of great significance in guiding the construction of similar projects.

This paper presents an analytical solution for analyzing the interaction between the surrounding rock and supports of a circular tunnel. The proposed solution can be used to analyze the mechanical response of the supports installed in stages and surrounding rock, which constructively considers the intermediate principal stress, dilatancy, and strain-softening characteristics of surrounding rock in the red sandstone stratum. After verifying the rationality of the analytical solution, taking Yangcheng Tunnel of Haoji Railway in China as the research object, the influence laws and sensitivity of design parameters on the supporting effect are systematically analyzed. Finally, the application effect of the staged support installation method is compared with that of the traditional method.

2. Mechanical Model of Interaction between Surrounding Rock and Supports

2.1 Evolution Process of Interaction between Surrounding Rock and Supports

There are two sources of support force p_i acting on the inner wall of the tunnel during excavation (Chu et al., 2021). One is the virtual support force p_f provided by the spatial effect of the tunnel face, the other is the support force p_s provided by the artificial support. Since the secondary lining is usually regarded as a safety reserve, the artificial support in this paper only refers to the primary support, including steel frame and shotcrete. The support forces provided by steel frames and shotcrete are defined as p_{set} and p_{shot}, respectively. In terms of the source and development trend of the support force acting on the inner wall of the tunnel, four main stages of the interaction process are determined in this paper, as shown in Fig. 1.

In stage a, the surrounding rock is not disturbed by tunnel construction, such as section $A-A'$, resulting in the total support force p_i acting on the inner wall is equal to the unaltered stress of the original rock σ_0; In stage b, the artificial support has not been installed, such as section $B-B'$, thus the support force is only provided by the tunnel face, that is, $p_i = p_f$; In stage c, the total support force p_i consists of p_f and p_s. When only the steel frames

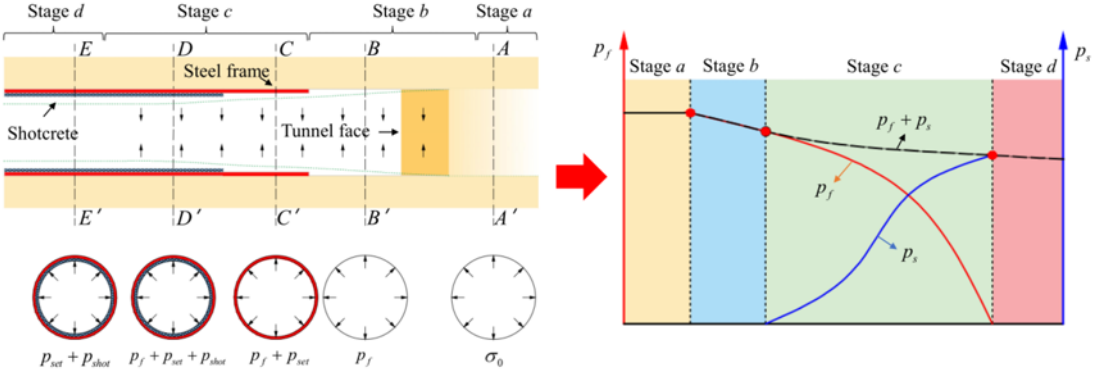

Fig. 1. Whole Process of the Interaction between Surrounding Rock and Supports

are installed, such as section $C-C'$, p_s equals to p_{set}. When both the steel frames and shotcrete are installed, such as section $D-D'$, p_s consists of p_{set} and p_{shot}, that is, $p_s = p_{set} + p_{shot}$; In stages b and c, p_s develops gradually with the increase of the distance between the target section and the tunnel face, while p_f decreases gradually; In stage d, which occurs when the spatial effect provided by the tunnel face has completely disappeared, such as section $E-E'$, resulting in the support force only comes from the artificial supports, and the surrounding rock is in balance with the artificial supports. Obviously, the values of p_f and p_s have been dynamic, which are closely related to the interaction state between the surrounding rock and supports. The quantitative methods of these two support forces will be discussed in this paper.

2.2 Mechanical Model and Strength Criterion

The longitudinal dimension of the tunnel is significantly greater than its transverse dimension. As such, the three-dimensional problem can be transformed into a plane strain problem. The mechanical model adopted for the tunnel is based on the following assumptions:

1. The surrounding rock mass is assumed to be isotropic, and is uniformly subjected to original rock stress σ_0;
2. The cross-sectional contour of the tunnel is circular, and the support force p_i conducted by the inner wall is uniformly distributed;
3. The plane section assumption is satisfied.

Previous studies have shown that red sandstone has strain-softening properties under external forces. With the continuous increase of strain, the rock mass will be followed by the elastic stage, plastic softening stage and residual stage (Wen et al., 2013; Zhou et al., 2018; Huang et al., 2020). Thus, during the construction progress, the disturbed rock outside the tunnel is susceptible to exhibiting different elastoplastic states, such as the elastic state, plastic softening state, or residual state, as illustrated in Fig. 2. R_0, R_p, and R_b represent the radius of the excavated zone, plastic softening zone, and residual zone, respectively. σ_θ, σ_r, and σ_z correspond to the tangential, radial, and axial stress, respectively. At the elastic-plastic boundary (point A), the tangential and radial stresses are respectively represented by σ_θ^{e-p} and σ_r^{e-p}, whereas at the boundary between the plastic softening zone and residual zone (point B), the tangential and radial stresses are represented by σ_θ^{e-b} and σ_r^{e-b}, respectively. Based on the mechanical model elucidated in Fig. 2, the equilibrium equation, geometric equation, and constitutive equation can be established as follows:

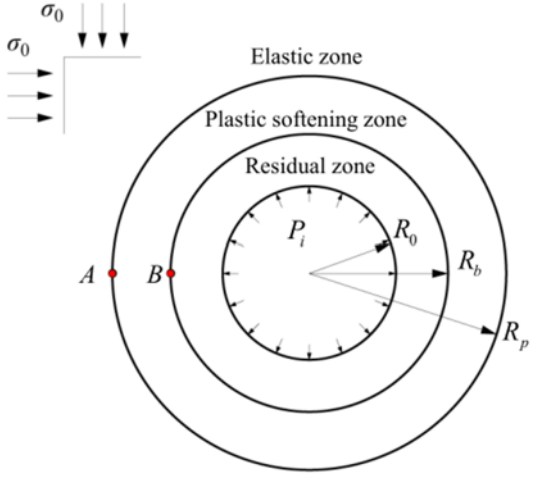

Fig. 2. Mechanical Model of a Circular Tunnel in the Transverse Direction

$$\frac{d\sigma_r}{dr}+\frac{\sigma_r-\sigma_\theta}{r}=0\,, \tag{1}$$

$$\varepsilon_r=\frac{du}{dr},\quad \varepsilon_\theta=\frac{u}{r},\quad \varepsilon_z=0\,, \tag{2}$$

$$\varepsilon_r=\frac{1-\nu^2}{E}\left(\sigma_r-\frac{\nu}{1-\nu}\sigma_\theta\right),\quad \varepsilon_\theta=\frac{1-\nu^2}{E}\left(\sigma_\theta-\frac{\nu}{1-\nu}\sigma_r\right). \tag{3}$$

For red sandstone, which has the property of strain softening formation, once the stress level of rock mass surpasses its compressive strength, the mechanical parameters associated with the rock mass will gradually diminish to their respective residual values with an increasing strain (Riabokon et al., 2021). Based on laboratory tests and mathematical analysis, Li et al. (2011) and Luo (2018) obtained the attenuation laws of the internal friction angle φ and cohesive c, as shown in Fig. 3, where φ_0 and φ^* refer to the internal friction angles of the surrounding rock in elastic and residual state, respectively. The attenuation law of the internal friction angle φ corresponding to the plastic softening stage is described as follows:

$$\varphi^p=A_0\left(\varepsilon_\theta^p-\varepsilon_\theta^{e-p}\right)^2+B_0\left(\varepsilon_\theta^p-\varepsilon_\theta^{e-p}\right)+C_0\,, \tag{4}$$

where A_0, B_0, and C_0 are constants.

From the boundary conditions $\varphi\left(\varepsilon_\theta^{e-p}\right)=\varphi_0$, $\varphi\left(\varepsilon_\theta^{p-b}\right)=\varphi^*$, and $\left(d\varphi/d\varepsilon^p\right)\big|_{\varepsilon^p=\varepsilon_\theta^{p-b}}=0$, the solution of φ^p can be obtained as follows:

$$\varphi^p=T_\varphi\left(\varepsilon_\theta^p-\varepsilon_\theta^{e-p}\right)^2\Big/\left(\varepsilon_\theta^{p-b}-\varepsilon_\theta^{e-p}\right)-2T_\varphi\left(\varepsilon_\theta^p-\varepsilon_\theta^{e-p}\right)+\varphi_0\,, \tag{5}$$

where T_φ is the softening modulus of φ, which $T_\varphi=(\varphi_0-\varphi^*)/\left(\varepsilon_\theta^{p-b}-\varepsilon_\theta^{e-p}\right)$.

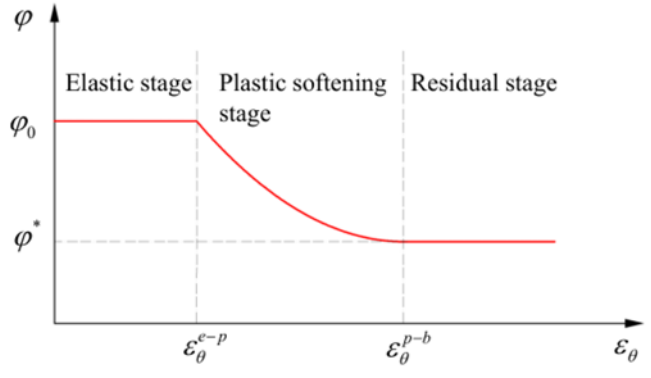

Fig. 3. Mechanical Parameter Attenuation Model of Surrounding Rock in Red Sandstone Stratum: Take Internal Friction Angle as an Example

Similarly, the solution of c^p can be obtained as Eq. (6).

$$c^p = T_c\left(\varepsilon_\theta^p - \varepsilon_\theta^{e-p}\right)^2 \Big/ \left(\varepsilon_\theta^{p-b} - \varepsilon_\theta^{e-p}\right) - 2T_c\left(\varepsilon_\theta^p - \varepsilon_\theta^{e-p}\right) + c_0 \quad (6)$$

Hu and Yu (2005) proposed an improved unified strength criterion that comprehensively considers the impact of all three stress couples operating on the principal shear planes of the dodecahedral element, thereby enabling reflection of the nonlinear strength characteristics of geomaterials. Yu et al. (2013) matched the conventional unified strength criterion to the well-known Drucker–Prager strength criterion, which enabled the reasonable integration of the intermediate principal stress. Herein, the improved unified strength criterion is matched with the Drucker-Prager strength criterion and the expression is as follows:

$$\left.\begin{aligned} f &= \sigma_\theta - m(\psi)\sigma_r - n(\psi) = 0 \\ m(\psi) &= \frac{1 - 3\alpha\alpha_\psi + 3\alpha\sqrt{1-3\alpha_\psi^2}}{1 - 3\alpha\alpha_\psi - 3\alpha\sqrt{1-3\alpha_\psi^2}} \\ n(\psi) &= \frac{2\kappa\sqrt{1-3\alpha_\psi^2}}{1 - 3\alpha\alpha_\psi - 3\alpha\sqrt{1-3\alpha_\psi^2}} \end{aligned}\right\}, \quad (7)$$

where α and κ can be obtained by Eq. (8); ψ is the dilatancy angle; α_ψ is the dilatancy parameter, which satisfies $\alpha_\psi = \alpha$ when $\psi = \varphi$ (Deng et al., 2009); $t = 3\alpha_\psi \Big/ \sqrt{1-3\alpha_\psi^2}$.

$$\left.\begin{aligned} \alpha &= \frac{bt^3(\sin\varphi - 1) + 8t\sin\varphi(b+1)}{3\alpha_\psi bt^3(\sin\varphi - 1) + 9\alpha_\psi bt^2(5 - \sin\varphi) + 24\alpha_\psi t\sin\varphi(b+1) + 36\alpha_\psi(b+2)} \\ \kappa &= \frac{8ct\cos\varphi(b+1)}{\alpha_\psi bt^3(\sin\varphi - 1) + 3\alpha_\psi bt^2(5 - \sin\varphi) + 8\alpha_\psi t\sin\varphi(b+1) + 12\alpha_\psi(b+2)} \end{aligned}\right\} \quad (8)$$

Based on the non-associated flow law (Bernaud and Quevedo, 2020), the relationship between the radial strain ε_r^p and the tangential strain ε_θ^p of the rock in the plastic zone can be described as follows:

$$d\varepsilon_r^p + \eta d\varepsilon_\theta^p = 0 , \quad (9)$$

where $\eta = -m(\psi)$.

2.3 Mechanical Characteristics of the Artificial Supports Installed in Stages

The primary support system in mountain tunnels predominantly comprises of the steel frames and shotcrete. In accordance with the new Austrian method, the flexibility of the artificial support system can be enhanced by adopting a staged installation procedure. This entails installing the steel frames and shotcrete at varying distances from the tunnel face, which are defined as x_{ini} and x_1, respectively, as shown in Fig. 4. Such an installation method is beneficial in mobilizing the self-bearing capacity of the surrounding rock and minimizing the likelihood of structural failures. It is evident that the flexibility of the support system that is installed in stages is principally influenced by the material parameters, geometric parameters, and initial install locations. It is of paramount importance to rationally determine the values of these parameters to attain the optimal balance between structural safety and deformation control efficacy.

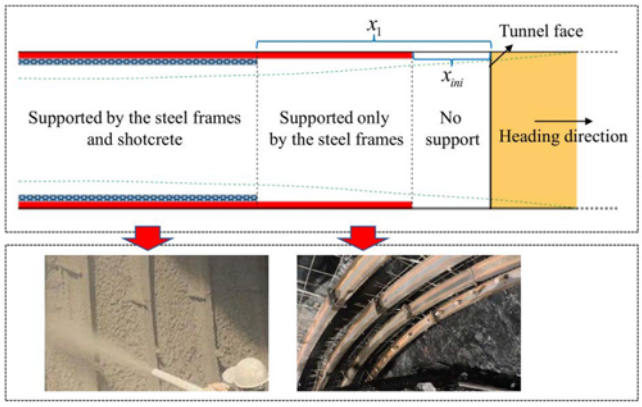

Fig. 4. Schematic of the Staged Installation of the Artificial Supports

Based on the thick-walled cylinder theory (Drescher and Detournay, 1993), the stiffness of the steel frames and shotcrete can be obtained by Eqs. (10) and (11), respectively.

$$k_{set} = \frac{A_{set}E_{set}}{d\left(R_0 - h_{set}/2\right)^2} , \quad (10)$$

where k_{set}, A_{set}, E_{set}, h_{set}, and d represent the stiffness, elastic modulus, equivalent thickness, Poisson's ratio, and spacing of the steel frames, respectively.

$$k_{shot} = \frac{E_{shot}\left[R_0^2 - \left(R_0 - d_{shot}\right)^2\right]}{R_0\left(1 + v_{shot}\right)\left[\left(1 - 2v_{shot}\right)R_0^2 + \left(R_0 - d_{shot}\right)^2\right]} , \quad (11)$$

where k_{shot}, E_{shot}, d_{shot}, and v_{shot} represent the stiffness, elastic modulus, equivalent thickness, and Poisson's ratio of the shotcrete, respectively.

In the case of staged support installation, the support force p_s can be obtained by Eq. (12). The equation comprises of two distinct parts: the first part indicates the stage supported solely by the steel frames whereas the latter denotes the stage supported by the conjunction of steel frames and shotcrete.

$$p_s = \begin{cases} k_{set}\left[u_{R_0}^{p_f + p_{set}}(x) - u_{R_0}^{p_f}(x_{ini})\right], & x_{ini} < x \le x_1 \\ k_{set}\left[u_{R_0}^{p_f + p_{set}}(x_1) - u_{R_0}^{p_f}(x_{ini})\right], \\ +\left(k_{set} + k_{shot}\right)\left[u_{R_0}^{p_f + p_{set} + p_{shot}}(x) - u_{R_0}^{p_f + p_{set}}(x_1)\right], & x \ge x_1 \end{cases} \quad (12)$$

where x represents the distance between the section and the tunnel face; $u_{R_0}^{p_0}$, $u_{R_0}^{p_f + p_{set}}$, and $u_{R_0}^{p_f + p_{set} + p_{shot}}$ represent the radial displacement of the surrounding rock during successive stages, namely: the stage without any support, the stage only supported by the steel frames, and the stage supported collectively by steel frames and shotcrete. It is pertinent to note that breaching the ultimate bearing capacity of any component should be regarded as an indicator of support system failure. Therefore, to maintain the normal functionality of the support system, it is necessary to ensure that Eq. (13) is satisfied.

$$\left.\begin{aligned} 0 \le k_{set}\left[u_{R_0}^{p_f+p_{set}+p_{shot}}(x)-u_{R_0}^{p_f}(x_{ini})\right] < p_{set}^{\max} \\ 0 \le k_{shot}\left[u_{R_0}^{p_f+p_{set}+p_{shot}}(x)-u_{R_0}^{p_f+p_{set}}(x_1)\right] < p_{shot}^{\max} \end{aligned}\right\}, \tag{13}$$

where $p_{set}^{\max}$ represents the ultimate bearing capacity of the steel frames and satisfies $p_{set}^{\max}=A_{set}\sigma_{set}\big/\left[d\left(R_0-h_{set}/2\right)\right]$; $p_{shot}^{\max}$ represents the ultimate bearing capacity of the shotcrete and satisfies $p_{shot}^{\max}=\sigma_{c,shot}\left[R_0^2-\left(R_0-d_{shot}\right)^2\right]\big/\left(2R_0^2\right)$.

2.4 Quantitative Method of Virtual Support Force

As one moves away from the tunnel face, the virtual support force acting on the inner wall diminishes continually, resulting in the progressive increase of the surrounding rock's radial displacement. It is possible to use the longitudinal deformation profile (LDP) of the tunnel without artificial support to assess the attenuation law of the virtual support force. Moreover, the ground reaction curve (GRC) can reflect the relationship between the support force and the surrounding rock's radial displacement. The coupling analysis method based on LDP and GRC is able to quantify the virtual support force. Previous research conducted by Vlachopoulos and Diederichs (2009) obtained the LDP expression founded on numerous finite difference simulations, which can be expressed as Eq. (14). As for the GRC expression, it should be established based on an elastoplastic analysis of the surrounding rock in the red sandstone stratum, as elaborated on in Section 3.0.

$$u_{R_0}^{p_f}(x)=\begin{cases} u_{R_0}(\infty)\cdot u_0^*\cdot\exp\left(x^*\right), & x\le 0 \\ u_{R_0}(\infty)\cdot\left[1-\left(1-u_0^*\right)\exp\left(-\dfrac{1.5x^*}{R^*}\right)\right], & x\ge 0, \end{cases} \tag{14}$$

where $u_{R_0}^{p_f}$ represents the radial displacement of the surrounding rock without artificial support; $u_{R_0}(\infty)$ represents the radial displacement when the virtual support force is zero; u_0^* is the displacement release coefficient at the tunnel face and satisfies $u_0^*=\exp(-0.15R^*)/3$; $R^*=R_p^{\max}/R_0$, $R_p^{\max}$ is the plastic radius when the virtual support force is zero; $x^*=x/R_0$.

3. Elastoplastic Analysis of the Surrounding Rock in the Red Sandstone Stratum

3.1 Solution of Elastic Zone

The stress at any point within the elastic zone σ^e, and the corresponding radial displacement u^e, can be determined using Eqs. (15) and (16), respectively.

$$\left.\begin{aligned} \sigma_r^e &= \sigma_0-\left(\sigma_0-\sigma_r^{e-p}\right)\left(\frac{R_p}{r}\right)^2 \\ \sigma_\theta^e &= \sigma_0+\left(\sigma_0-\sigma_r^{e-p}\right)\left(\frac{R_p}{r}\right)^2 \end{aligned}\right\}, \tag{15}$$

$$u^e=\frac{\left(\sigma_0-\sigma_r^{e-p}\right)R_p^2}{2Gr},\quad G=\frac{E}{2(1+\nu)} \tag{16}$$

where G represents the shear modulus.

The radial stress at the elastic-plastic boundary σ_r^{e-p} can be obtained by substituting Eq. (1) into the yield criterion Eq. (7).

$$\sigma_r^{e-p}=\frac{2\sigma_0-n^{e-p}}{1+m^{e-p}} \tag{17}$$

3.2 Solution of Plastic Softening Zone

The strain of the surrounding rock in the plastic softening zone ε^p consists of elastic strain ε^{pe} and plastic strain ε^{pp}, that is, $\varepsilon_r^p=\varepsilon_r^{pe}+\varepsilon_r^{pp}$, $\varepsilon_\theta^p=\varepsilon_\theta^{pe}+\varepsilon_\theta^{pp}$. From Eq. (9), the following is obtained:

$$\varepsilon_r^p+\eta_1\varepsilon_\theta^p=\varepsilon_r^{pe}+\eta_1\varepsilon_\theta^{pe}, \tag{18}$$

where $\eta_1=m\left(\psi^p\right)$, ψ^p refers to the dilatancy angle of the rock in the plastic softening zone.

Combining the boundary conditions $\varepsilon_r^{pe}=\varepsilon_r^e\left(r=R_p\right)$, $\varepsilon_\theta^{pe}=\varepsilon_\theta^e\left(r=R_p\right)$, the following can be obtained by substituting Eq. (2) into Eq. (18).

$$\frac{du^p}{dr}+\eta_1\frac{u^p}{r}=\frac{1+\nu}{E}(\eta_1-1)\left(\sigma_0-\sigma_r^{e-p}\right) \tag{19}$$

From the boundary condition $u^p\left(r=R_p\right)=u^e\left(r=R_p\right)$, the radial displacement of the surrounding rock in the plastic softening zone u^p can be obtained as follows:

$$u^p=\frac{r\left(\sigma_0-\sigma_r^{e-p}\right)}{2G\left(1+\eta_1\right)}\left[\eta_1-1+2\left(\frac{R_p}{r}\right)^{\eta_1+1}\right]. \tag{20}$$

Based on the boundary condition $\sigma_r^p\left(r=R_p\right)=\sigma_r^{e-p}\left(r=R_p\right)+\eta_1\varepsilon_\theta^{pe}$, the stress in the plastic softening zone σ^p can be obtained by substituting Eq. (7) into Eq. (15).

$$\left.\begin{aligned} \sigma_r^p &= \left(\sigma_r^{e-p}+\frac{n^p}{m^p-1}\right)\left(\frac{r}{R_p}\right)^{m^p-1}-\frac{n^p}{m^p-1} \\ \sigma_\theta^p &= m^p\left(\sigma_r^{e-p}+\frac{n^p}{m^p-1}\right)\left(\frac{r}{R_p}\right)^{m^p-1}-\frac{n^p}{m^p-1} \end{aligned}\right\} \tag{21}$$

3.3 Solution of Residual Zone

Based on the boundary condition $\sigma_r^b\left(r=R_0\right)=p_i$, the stress in the residual zone σ^b can be obtained by substituting Eq. (7) into Eq. (15).

$$\left.\begin{aligned} \sigma_r^b &= \left(p_i+\frac{n^b}{m^b-1}\right)\left(\frac{r}{R_0}\right)^{m^b-1}-\frac{n^b}{m^b-1} \\ \sigma_\theta^b &= m^b\left(p_i+\frac{n^b}{m^b-1}\right)\left(\frac{r}{R_0}\right)^{m^b-1}-\frac{n^b}{m^b-1} \end{aligned}\right\} \tag{22}$$

Combine the generalized Hook law (Guo et al., 2022) and Eq. (18), the following is obtained:

$$\frac{du^b}{dr}+\eta_2\frac{u^b}{r}=\varepsilon_r^{be}+\eta_2\varepsilon_\theta^{be}=\frac{\sigma_r^b-\nu\left(\sigma_\theta^b+\sigma_z^b\right)}{E}+\eta_2\frac{\sigma_\theta^b-\nu\left(\sigma_r^b+\sigma_z^b\right)}{E}, \tag{23}$$

where $\eta_2 = m(\psi^b)$, ψ^b refers to the dilatancy angle of the rock in the residual zone.

From the boundary condition $u^b(r=R_b) = u^p(r=R_b)$, the radial displacement of the surrounding rock in the residual zone u^b can be obtained as follows:

$$u^b = \frac{R_b^{\eta_2+1}\left(\sigma_0 - \sigma_r^{e-p}\right)}{2G(\eta_1+1)r^{\eta_2}}\left[\eta_1 - 1 + 2\left(\frac{R_p}{R_b}\right)^{\eta_1+1}\right] - \frac{\chi_1\left(R_b^{\eta_2+m^b} - r^{\eta_2+m^b}\right)}{R_0^{m^b-1}\left(\eta_2+m^b\right)r^{\eta_2}} + \frac{\chi_2\left(R_b^{\eta_2+1} - r^{\eta_2+1}\right)}{(\eta_2+1)r^{\eta_2}}, \tag{24}$$

where $\chi_1 = \frac{\nu(\eta_2 m^b - 3\eta_2 - 3m^b) + \nu(1+\eta_2)(1-m^b)t^b}{2E}\left(p_i + \frac{n^b}{m^b-1}\right)$,

$\chi_2 = \frac{(1+\eta_2)(1-2\nu)}{E}\frac{n^b}{m^b-1}$.

3.4 Solution of Plastic Radius in the Plastic Zone

From the boundary condition $\sigma_r^b(r=R_b) = \sigma_r^p(r=R_b)$, the radius of the plastic softening zone R_p can be obtained as follows:

$$R_p = \sqrt[m^b-1]{\frac{\left(m^b-1\right)\sigma_r^{e-p} + n^b}{\left(m^b-1\right)P_i + n^b}} \cdot R_0 . \tag{25}$$

The internal friction angle of the surrounding rock in the residual zone φ^* is constant. From Eq. (5), the expression of φ^* is as follows:

$$\varphi^* = \varphi_0 - T_\varphi \frac{\left(\sigma_0 - \sigma_r^{e-p}\right)}{G(1+\eta_1)}\left[\left(\frac{R_p}{R_b}\right)^{\eta_1+1} - 1\right]. \tag{26}$$

Combine Eqs. (25) and (26), the radius of the residual zone R_b is obtained:

$$R_b = R_p\left[1 + \frac{G(\varphi_0 - \varphi^*)(1+\eta_1)}{T_\varphi\left(\sigma_0 - \sigma_r^{e-p}\right)}\right]^{-\frac{1}{1+\eta_1}}, \tag{27}$$

4. Analytical Solution of Interaction between Surrounding Rock and Support

4.1 Judge Theorem of the Interaction States and Corresponding Solution Formulas

The interaction between the surrounding rock and supports is continuously dynamic. To account for the elastoplastic state of the surrounding rock and the progress of artificial support installation, six interaction states are proposed, as shown in Fig. 5.

The progress of artificial support installation can be determined by examining the relationship between x, x_{ini}, and x_1. When $x < x_{ini}$, the surrounding rock is not supported; When $x_{ini} < x < x_1$, the surrounding rock is only supported by the steel frames; When $x > x_1$, the surrounding rock is collectively supported by the steel frames and shotcrete. When the inner wall is the boundary of the elastic zone, that is, $R_p = R_0$, the corresponding threshold support force is defined as $p_{\lim}^{e-p}$, which is equivalent to σ_r^{e-p}. The expression of $p_{\lim}^{e-p}$ is shown as Eq. (28). When the inner wall is the boundary of the residual zone, that is, $R_b = R_p$, the corresponding threshold support force is defined as $p_{\lim}^{p-b}$. From Eq. (27), the solution of $p_{\lim}^{p-b}$ can be obtained as Eq. (29). Hence, when $p_i \geq p_{\lim}^{e-p}$, the surrounding rock of the inner wall is in the elastic state; When $p_{\lim}^{p-b} \leq p_i < p_{\lim}^{e-p}$, the surrounding rock of the inner wall is in the plastic softening state; When $p_i < p_{\lim}^{p-b}$, the surrounding rock of the inner wall is in the residual state.

$$p_{\lim}^{e-p} = \frac{2\sigma_0 - n^{e-p}}{1+m^{e-p}} \tag{28}$$

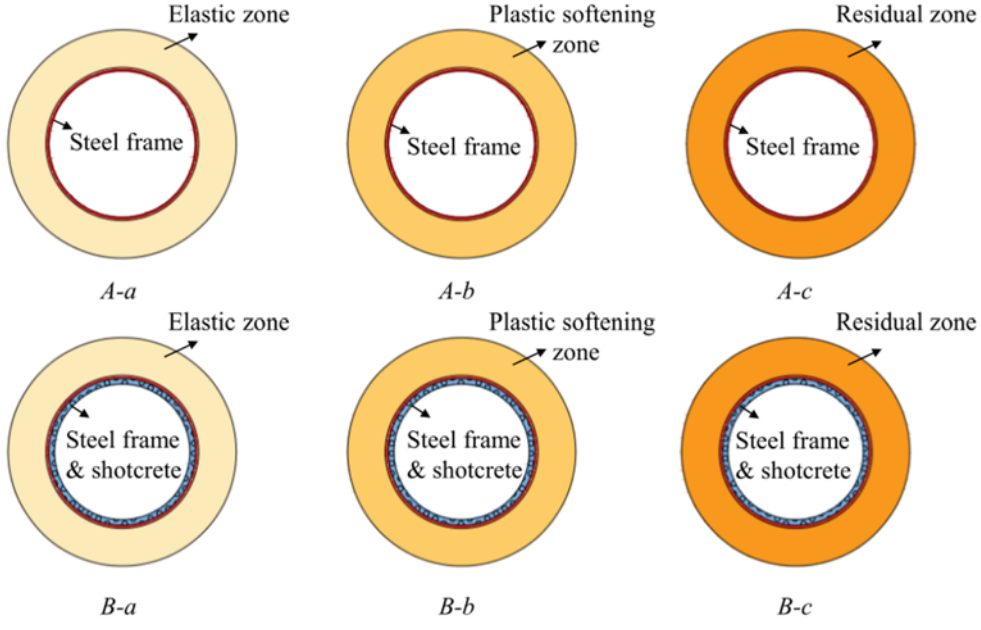

Fig. 5. Types of Interaction States between Surrounding Rock and Supports

$$p_{\lim}^{p-b}=\frac{\left(m^b-1\right)\sigma_r^{e-p}+n^b}{\left(m^b-1\right)\left[1+\frac{G\left(\varphi_0-\varphi^*\right)\left(1+\eta_1\right)}{T_\varphi\left(\sigma_0-\sigma_r^{e-p}\right)}\right]^{\frac{m^b-1}{1+\eta_1}}}-\frac{n^b}{m^b-1} \tag{29}$$

When the inner wall is only supported by the steel frames ($x_{ini}<x<x_1$), the solution formula of the artificial support force $p_s(x)$ is as Eq. (30). Ulteriorly, considering the elastoplastic state of surrounding rock, three types of interaction between surrounding rock and supports (numbered as A-a, A-b, and A-c) can be proposed.

$$p_s(x)=k_{set}\left[u_{R_0}^{p_f+p_{set}}(x)-u_{R_0}^{p_f}\left(x_{ini}\right)\right] \tag{30}$$

For state A-a, the radial displacement of the inner wall $u_{R_0}^{p_f+p_{set},e}$ can be obtained through the coupling analysis of GRC and SRC. This can be achieved by substituting Eq. (30) into Eq. (16).

$$u_{R_0}^{p_f+p_{set},e}(x)=\frac{\left[\sigma_0-p_f^e(x)+k_{set}u_{R_0}^{p_f}\left(x_{ini}\right)\right]\cdot R_0}{2G+k_{set}R_0} \tag{31}$$

Similarly, for state A-b, the radial displacement $u_{R_0}^{p_f+p_{set},p}$ can be attained by the simultaneous solution of Eqs. (20), (21), and (30).

$$u_{R_0}^{p_f+p_{set},p}(x)=\frac{\sigma_0\left(\frac{R_0}{R_p}\right)^{m^p-1}+\left[\left(\frac{R_0}{R_p}\right)^{m^p-1}-1\right]\cdot\frac{n^p}{m^p-1}-p_f^p(x)+k_{set}u_{R_0}^{p_f}\left(x_{ini}\right)}{\frac{1}{\omega}\left(\frac{R_0}{R_p}\right)^{m^p-1}+k_{set}} \tag{32}$$

where $\omega=\frac{R_0}{2G\left(1+\eta_1\right)}\left[\eta_1-1+2\left(\frac{R_p}{R_0}\right)^{\eta_1+1}\right]$.

For state A-c, the radial displacement $u_{R_0}^{p_f+p_{set},b}$ can be obtained by the simultaneous solution of Eqs. (22), (24), and (30).

$$u_{R_0}^{p_f+p_{set},b}(x)=\frac{\xi_1\left[p_f^b(x)-k_{set}u_{R_0}^{p_f}\left(x_{ini}\right)+\frac{n^b}{m^b-1}\right]+\xi_2}{R_0^{\eta_2}-k_{set}\xi_1} \tag{33}$$

where

$$\xi_1=\frac{\chi_1\left(R_0^{\eta_2+1}-R_b^{\eta_2+1}\right)}{\left(p_i+\frac{n^b}{m^b-1}\right)\left(\eta_2+m^b\right)},\quad \xi_2=\frac{\chi_2\left(R_0^{\eta_2+1}-R_b^{\eta_2+1}\right)}{\eta_2+1}+\frac{\omega R_b^{\eta_2+1}\left(\sigma_0-\sigma_r^{e-p}\right)}{R_0\left(\eta_1+1\right)}.$$

Herein, $p_f^e(x)$, $p_f^p(x)$, and $p_f^b(x)$ respectively correspond to the virtual support force acting on the inner wall in the elastic state, plastic softening state, and residual state. By substituting Eq. (14) into the expressions of GRC associated with various elastoplastic stages, i.e., Eqs. (16), (20), and (24), the solutions of $p_f^e(x)$, $p_f^p(x)$, and $p_f^b(x)$ can be ascertained as follows:

$$p_f^e(x)=\sigma_0-\frac{2G\cdot u_{R_0}^{p_f}}{R_0}, \tag{34}$$

$$p_f^p(x)=\left\{\sigma_0-\frac{1}{\omega}\cdot u_{R_0}^{p_f}(x)+\frac{n^p}{m^p-1}\right\}\cdot\left(\frac{R_0}{R_p}\right)^{m^p-1}-\frac{n^p}{m^p-1}, \tag{35}$$

$$p_f^b(x)=\frac{u_{R_0}^{p_f}(x)\cdot R_0^{\eta_2}-\xi_2}{\xi_1}-\frac{n^b}{m^b-1}. \tag{36}$$

When the inner wall is supported by the steel frames and shotcrete together ($x>x_1$), the solution formula of the artificial support force $p_s(x)$ is as Eq. (37). Ulteriorly, taking into account the elastoplastic state of the surrounding rock, three types of interaction between surrounding rock and support can be proposed, which are numbered as B-a, B-b, and B-c. For each interaction type, the analytical solution for radial displacement of the inner wall can be determined as Eqs. (38), (39), and (40), respectively, and the derivation process is analogous to that detailed previously.

$$p_s(x)=k_{set}\cdot\tau+\left(k_{set}+k_{shot}\right)\left[u_{R_0}^{p_f+p_{set}+p_{shot}}(x)-u_{R_0}^{p_f+p_{set}}\left(x_1\right)\right] \tag{37}$$

where $\tau=k_{set}\left[u_{R_0}^{p_f+p_{set}}\left(x_1\right)-u_{R_0}^{p_f}\left(x_{ini}\right)\right]$.

$$u_{R_0}^{p_f+p_{set}+p_{shot},e}(x)=\frac{\left[\sigma_0-p_f^e(x)-k_{set}\cdot\tau+\left(k_{set}+k_{shot}\right)u_{R_0}^{p_f+p_{set},e}\left(x_1\right)\right]R_0}{2G+\left(k_{set}+k_{shot}\right)R_0} \tag{38}$$

$$u_{R_0}^{p_f+p_{set}+p_{shot},p}(x)=\frac{1}{\frac{1}{\omega}\left(\frac{R_0}{R_p}\right)^{m^p-1}+k_{set}+k_{shot}}\left\{\sigma_0\left(\frac{R_0}{R_p}\right)^{m^p-1}-p_f^p(x)+\left[\left(\frac{R_0}{R_p}\right)^{m^p-1}-1\right]\cdot\frac{n^p}{m^p-1}-k_{set}\cdot\tau+\left(k_{set}+k_{shot}\right)u_{R_0}^{p_f+p_{set},p}\left(x_1\right)\right\} \tag{39}$$

$$u_{R_0}^{p_f+p_{set}+p_{shot},b}(x)=\frac{\xi_1\left[p_f^b(x)+k_{set}\cdot\tau-\left(k_{set}+k_{shot}\right)u_{R_0}^{p_f+p_{set},b}\left(x_1\right)+\frac{n^b}{m^b-1}\right]+\xi_2}{R_0^{\eta_2}-\left(k_{set}+k_{shot}\right)\xi_1} \tag{40}$$

4.2 Analytical Solution of the Whole Process of Interaction between Surrounding Rock and Support

Combined with the analysis of the evolution process of interaction between surrounding rock and supports in Section 2.1, the analytical solution is established as follows:

1. Conduct an elastoplastic analysis of the surrounding rock in the red sandstone stratum based on the improved unified strength criterion and considers the influence of intermediate principal stress, dilatancy, and nonlinear strain-softening characteristics. Establish the relationship between the support force and radial displacement (GRC) as $u_{R_0}^{p_f}=f(p_i)$; Additionally, select an appropriate longitudinal deformation profile (LDP) as $u_{R_0}^{p_f}=g(x)$.
2. Assume the steel frames and shotcrete are installed at distances x_{ini} and x_1, respectively, from the tunnel face; The distance between the selected section and the tunnel face is $x=n\cdot v$; The advance rate is v; Days of construction is n. The installation progress of artificial support is divided into three stages based on the values of x, x_{ini}, and x_1: unsupported ($x<x_{ini}$), supported by the steel frames ($x_{ini}\le x<x_1$), and

supported by the steel frames and shotcrete ($x \geq x_1$).

When $x \geq x_1$, the resulting support characteristic curve (SRC) becomes the most complex in forms. The expression of the SRC in this case is as follows:

$$p_s(x) = k_{set}\left[u_{R_0}^{p_f+p_{set}}(x_1) - u_{R_0}^{p_f}(x_{ini})\right] + (k_{set}+k_{shot})\left[u_{R_0}^{p_f+p_{set}+p_{shot}}(x) - u_{R_0}^{p_f+p_{set}}(x_1)\right]. \quad (41)$$

Therefore, the following section only outlines the analytical steps that apply when the tunnel supports are comprised of both steel frames and shotcrete.

3. Assume that the surrounding rock is in a certain elastoplastic state, and obtain the virtual support at a distance of x_1 from the tunnel face $p_f(x_1) = f^{-1}[g(x_1)]$ by conducting a coupling analysis of GRC and LDP. This involves the simultaneous solution of $u_{R_0}^{p_f} = f(p_f)$ and $u_{R_0}^{p_f} = g(x_1)$. Subsequently, obtain the support force $p_{set}(x_1)$ and radial displacement $u_{R_0}^{p_f+p_{set}}(x_1)$ by conducting a coupling analysis of GRC and SRC. This involves the simultaneous solution of $u_{R_0}^{p_f+p_{set}} = f(p_f+p_{set})$ and $p_{set}(x_1) = k_{set}\cdot\left[u_{R_0}^{p_f+p_{set}}(x_1) - u_{R_0}^{p_f}(x_{ini})\right]$.
4. Calculate the total support force acting on the inner wall using $p_i(x_1) = p_f(x_1) + p_{set}(x_1)$, and confirm the correctness of the assumed elastoplastic state in step (c) using the judge theorem proposed in this paper. If the assumed state is correct, proceed to the subsequent steps. If not, select a new elastoplastic state and repeat steps (c) and (d).
5. Adjust the expression of SRC in step (c) from $p_{set}(x_1) = k_{set}\cdot\left[u_{R_0}^{p_f+p_{set}}(x_1) - u_{R_0}^{p_f}(x_{ini})\right]$ to $p_{set+shot}(x) = p_{set}(x_1) + (k_{set}+k_{shot})\cdot\left[u_{R_0}^{p_f+p_{set}+p_{shot}}(x) - u_{R_0}^{p_{set}}(x_1)\right]$, and determine the values of $p_f(x)$, $p_{set+shot}(x)$, and $u_{R_0}^{p_{set}+p_{shot}}(x)$ based on the methodology used in steps (c) and (d),
6. Use Eq. (13) to determine whether the failure of the artificial support has occurred. If it has, stop the calculation. If not, continue to step (g).
7. Determine whether the surrounding rock is balanced with the support according to whether $p_f(x)$ approaches zero. If it does, stop the calculation. If not, adjust $n = n+1$ and repeat steps (b) – (g).

The above solution process can be implemented through MATLAB programming, and the flowchart representation is presented in Fig. 6. By utilizing this program, the mechanical response of both the surrounding rock and the installed support

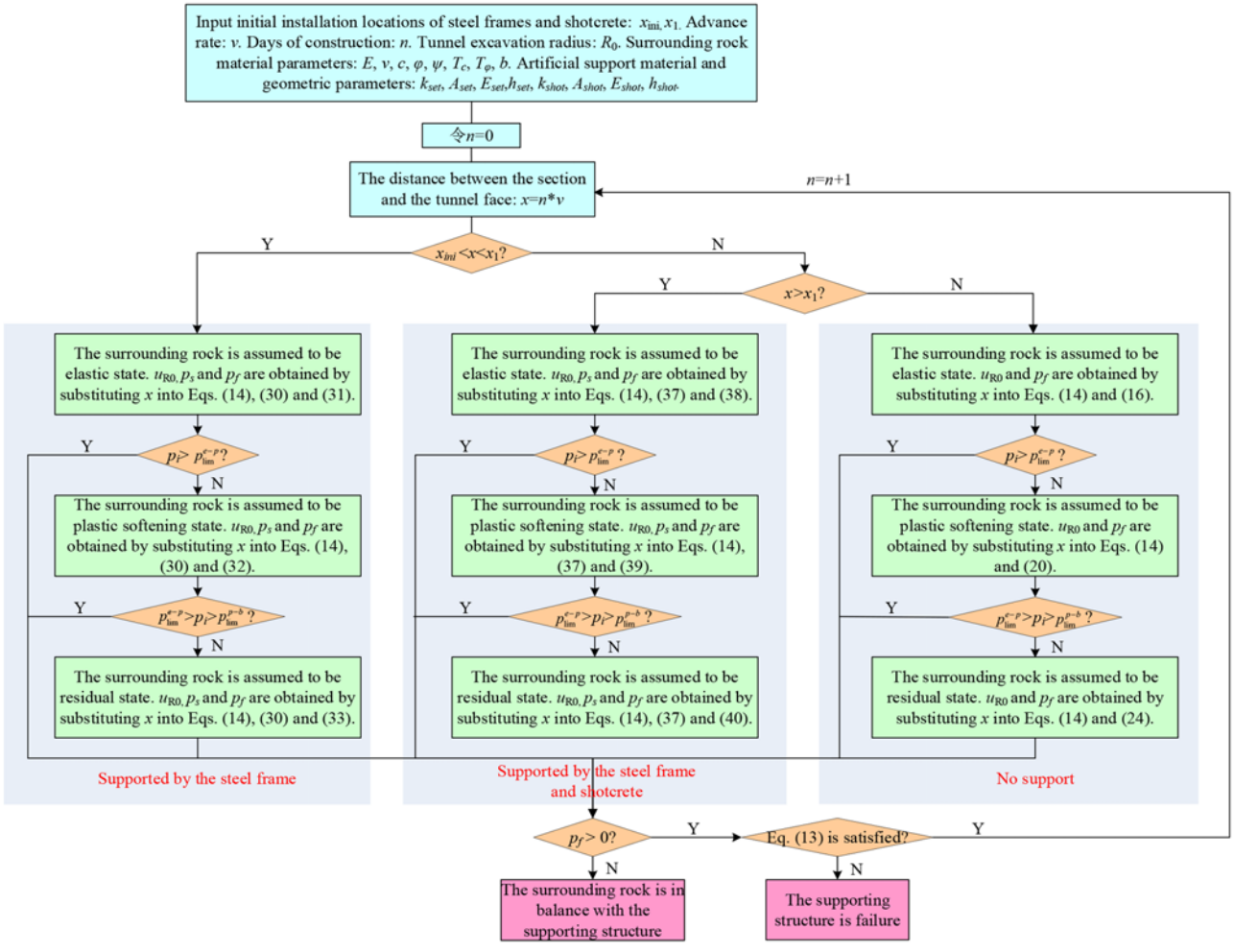

Fig. 6. Solution Process

system can be quantitatively assessed, which has a positive significance for controlling the flexibility of the support system.

5. Validation of the Analytical Solution

This section aims to validate the reliability and effectiveness of the proposed analytical solution by utilizing the Yangcheng Tunnel of Haoji Railway in the red sandstone stratum, shown in Fig. 7, as the research object. Detailed parameters of the surrounding rock and supports are listed in Tables 1 – 3. The approximate tunnel radius R_0, obtained via the equivalent circle method (Duan et al., 2023), is 5.8 m. Steel frame type I20 and shotcrete type C25 are used in this tunnel. The support stiffness and ultimate bearing capacity are calculated using Eqs. (10) – (13).

To validate the proposed analytical solution, a comparison is made with a previous solution. Fig. 8 shows the radial displacement curves obtained from the solutions proposed by this paper and Zhang et al. (2012). Note that the previous solution, based on the unified strength theory (Yu, 1994), cannot fully consider the stress characteristics of the rock mass and the nonlinear attenuation characteristics of the rock strength parameters.

The development trend of the rock radial displacement distribution curves obtained by the two methods is similar, with

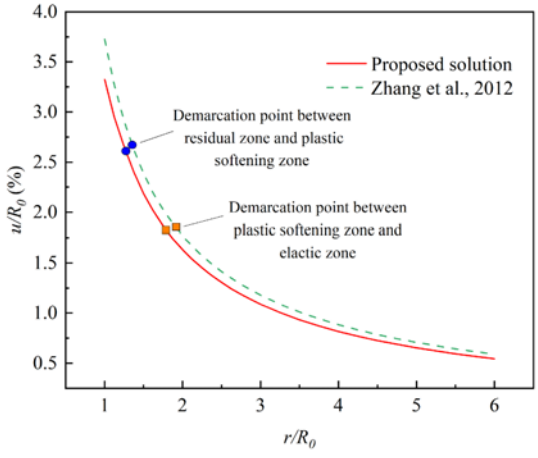

Fig. 8. Comparison of the Radial Displacement Curves of Surrounding Rock Obtained by Two Methods

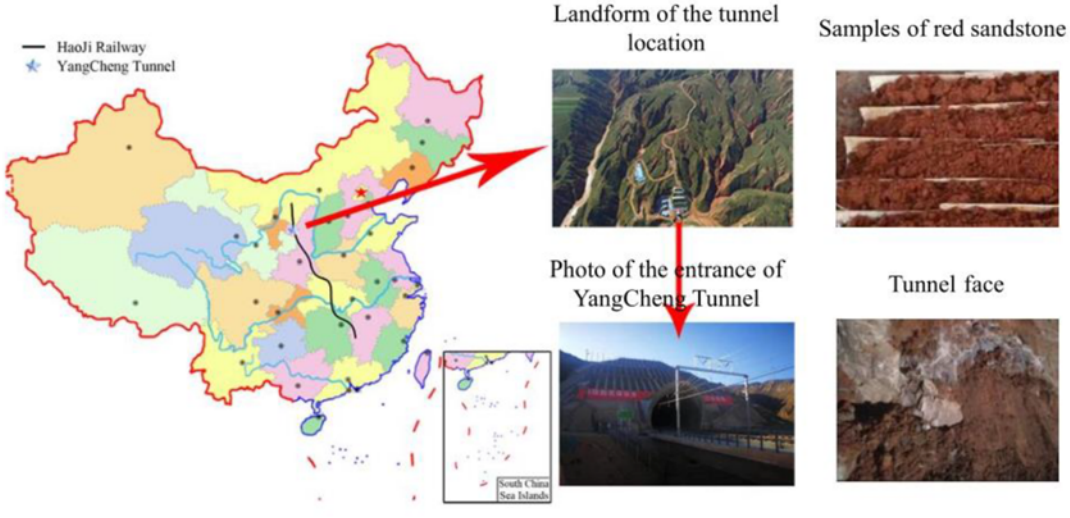

Fig. 7. Tunnel Engineering in Red Sandstone Stratum: Yangcheng Tunnel

Table 1. Parameters of Surrounding Rock

E (MPa)	ν	c_0 (MPa)	c^* (MPa)	φ_0 (8)	φ^* (8)	ψ^p (8)	ψ^b (8)	T_c (MPa)	T_φ (8)	σ_0 (MPa)	b
280	0.3	0.18	0.15	36	24	4.5	2.25	3	1,200	3.0	0.5

Table 2. Parameters of Steel Frame

A_{set} (cm^2)	h_{set} (m)	d (m)	k_{set} (MPa/m)	p_{set}^{max} (MPa)	E (GPa)	v	σ_c (MPa)
35.5	0.2	0.4	57.4	0.467	210	0.3	300

Table 3. Parameters of Shotcrete

d_{shot} (m)	k_{shot} (MPa/m)	p_{shot}^{max} (MPa)	E (GPa)	ν	σ_c (MPa)
0.37	276.4	1.040	23	0.2	17

main differences arising in the residual zone. The radius of residual zone and plastic softening zone obtained by the proposed method are 1.28 R_0 and 1.78 R_0, respectively, which are 5.9% and 7.3% smaller, respectively, than those obtained by Zhang et al. (2012). By and large, the application of the solution proposed by Zhang et al. (2012), overestimates the radial displacement of the surrounding rock. This observation indicates that the previous solution may result in a conservative engineering design, which can be attributed to its deficiencies in accounting for the intermediate principal stress, dilatancy, and strain-softening characteristics of the surrounding rock. In conclusion, the results obtained by the proposed analytical solution are more accurate than the previous solution.

6. Parametric Analysis

When the staged support installation method is employed, the mechanical response of the structure and surrounding rock during tunnel construction is affected by the initial install location and stiffness of each type of support. As such, this section conducts a parametric analysis to clarify their impact on surrounding rock deformation and support stress, which can aid in precisely controlling the flexibility of the support system.

As detailed in Section 2.3, on the premise that the material and geometric parameters of the artificial support remain constant, the initial install locations of the steel frames and shotcrete (designated as x_{ini} and x_1) will have a significant effect on the support flexibility of the supports. To investigate the impact of the initial install locations of the steel frames and shotcrete on the support flexibility, multiple calculation cases are established, as indicated in Table 4. The other parameters remain the same as those presented in Section 5.0.

Table 4. Calculation Cases of the Initial Install Location of the Supports

Analysis type	Non-variables	Variables
Analysis on the influence of the initial install location of the steel frames	$x_1 = 4$ m	$x_{ini} = 0, 1, 2, 3, 4$ m
Analysis on the influence of the initial install location of the shotcrete	$x_{ini} = 0$ m	$x_1 = 0, 2, 4, 6$ m

6.1 Influence of the Initial Install Location of the Steel Frame

Figure 9 displays the support stress development curves for various initial install locations of the steel frame x_{ini}.

Figure 9(a) shows that the stress development of the steel frame changes from rapid to basic stability after the shotcrete is installed. As x_{ini} increases from 0 to 4 m, the final stress value of the steel frame decreases from 0.275 to 0.088 MPa. This phenomenon demonstrates that postponing the initial install location of the steel frame can effectively reduce the final stress and improve the safety performance of the support structure; Fig. 9(b) shows that the stress development curve of the shotcrete is smoother than that of the steel frame. Increasing x_{ini} from 2 to 3 m shifts the surrounding rock from the plastic softening state to the residual state, resulting in an increase in the final shotcrete stress value from 0.129 to 0.168 MPa. This phenomenon indicates the excessive postponement of the support installation may cause the surrounding rock to shift into the residual state, generating additional pressure that may compromise structural safety.

Figure 10 displays the load sharing ratio and safety factor of the supports for varying x_{ini}.

As seen in Fig. 10, the load sharing ratios of the steel frame decrease as x_{ini} increases. When x_{ini} does not exceed 1 m, the steel frame is the primary bearing component of the artificial support system. When x_{ini} exceeds 4 m, the load sharing ratio of the shotcrete becomes about 5 times that of the steel frame. Increasing x_{ini} leads to a significant increase in the safety factor of the steel frame, whereas the safety factor of the shotcrete decreases.

Figure 11 shows the longitudinal distribution of the radial displacement of the inner tunnel wall for varying x_{ini}.

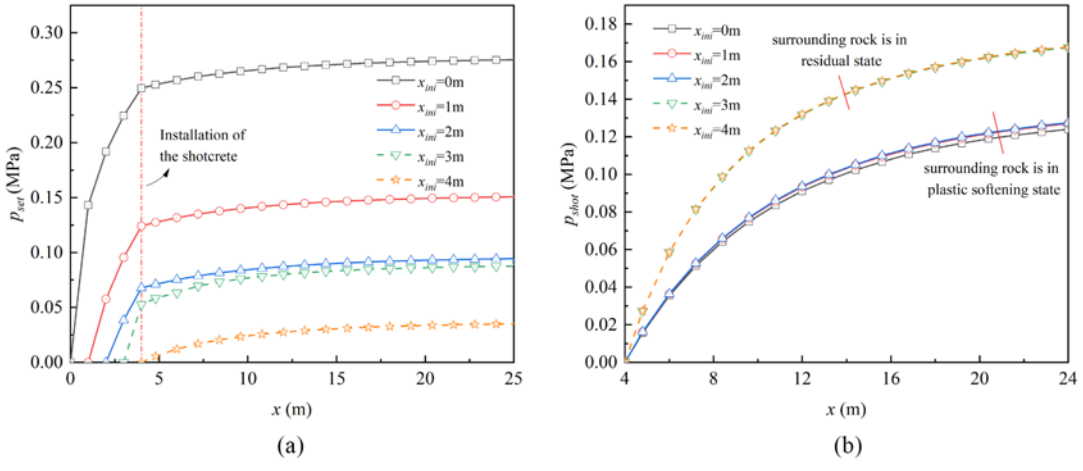

Fig. 9. Support Stress Development Curves for Varying x_{ini}: (a) Steel Frame Stress, (b) Shotcrete Stress

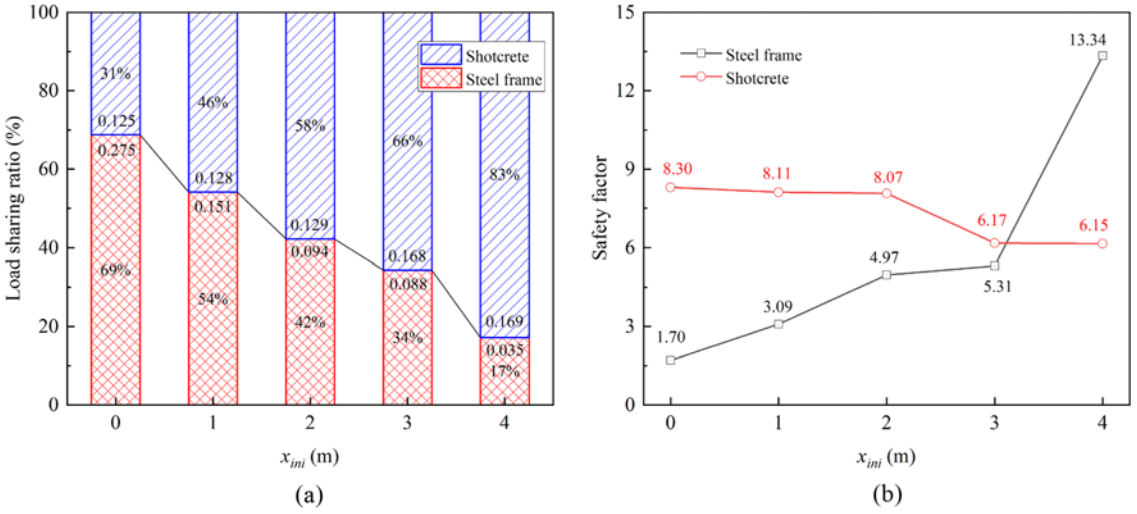

Fig. 10. Load Sharing Ratio and Safety Factor of the Supports for Varying x_{ini}: (a) Load Sharing Ratio, (b) Safety Factor

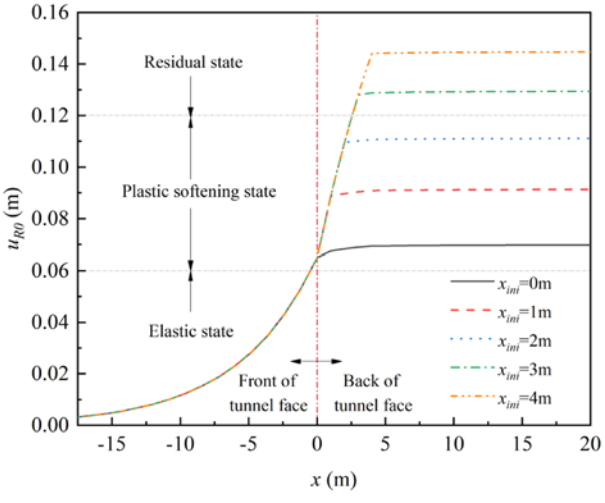

Fig. 11. Radial Displacement of the Inner Wall of the Tunnel for Varying x_{ini}

The radial displacement of the surrounding rock at the inner wall of the tunnel mainly develops between 1.3 times the tunnel span ahead of the tunnel face and 0.7 times the tunnel span behind the tunnel face. At the tunnel face, the radial displacement of the surrounding rock, which has entered the plastic softening state, is 65.0 mm. This demonstrates that the advanced core soil in the red sandstone stratum has poor natural strength. However, following the installation of the steel frame, convergence deformation of the surrounding rock is immediately brought under control. Increasing x_{ini} from 0 to 4 m causes the total radial displacement of the surrounding rock to increase from 69.7 to 144.7 mm. This demonstrates that the rock deformation is highly sensitive to the initial install location of the steel frame.

6.2 Influence of the Initial Install Location of the Shotcrete

Figure 12 shows the support stress development curves for

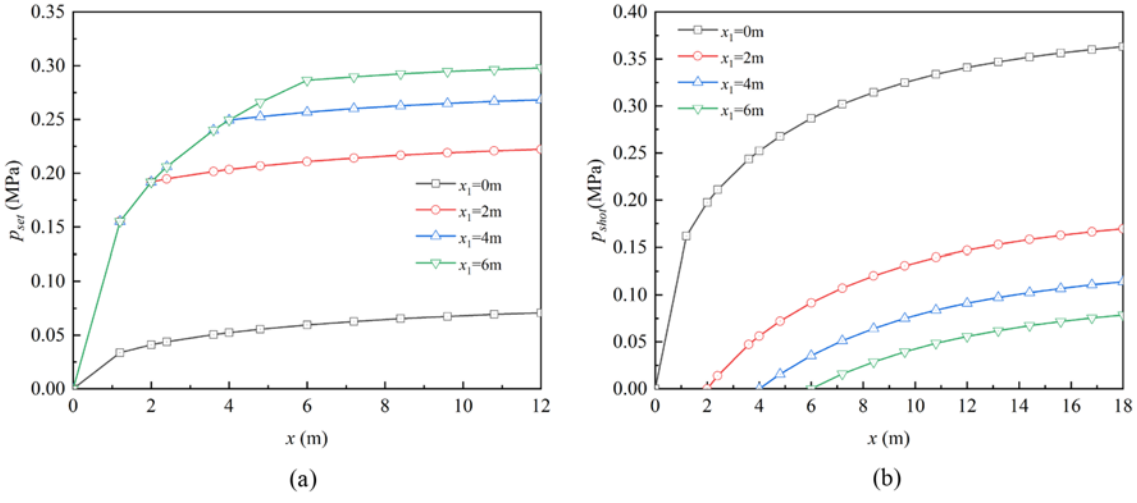

Fig. 12. Support Stress Development Curves for Varying x_1: (a) Steel Frame Stress, (b) Shotcrete Stress

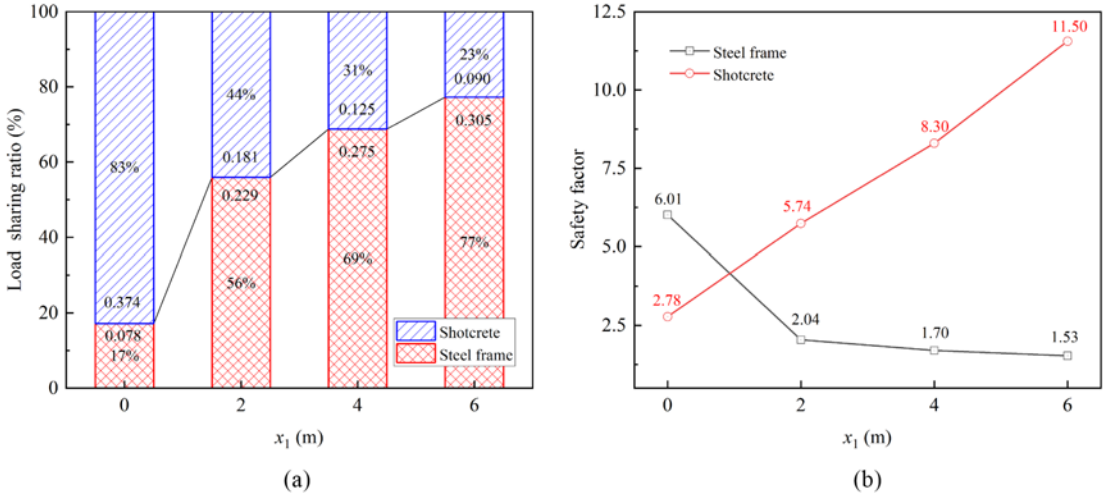

Fig. 13. Load Sharing Ratio and Safety Factor of the Supports for Varying x_1: (a) Load Sharing Ratio, (b) Safety Factor

varying initial install locations of the shotcrete x_1.

After the installation of the shotcrete, the stress development of the steel frame is immediately suppressed, while that of the shotcrete develops smoothly. When x_1 increases from 0 to 6 m, the amplitude of the steel frame stress is 0.193, 0.056, and 0.036 MPa, and the amplitude of the shotcrete stress is 0.193, 0.056, and 0.036 MPa. This indicates that the initial install location of the shotcrete, particularly with respect to its proximity to the tunnel face, has a significant impact on the amplitude of the structural stress.

Figure 13 shows the load sharing ratio and safety factor of the supports for varying x_1.

Increasing x_1 causes a gradual increase in the load sharing ratio of the steel frame, accompanied by a sharp decrease in its safety factor. It should be noted that the analytical solution presented in this paper does not account for the impact of hardening properties or installation quality on concrete strength. As a result, the actual safety factor of the steel frame may be lower than the calculated values shown in Fig. 13. This indicates that the staged installation method imposes strong requirements on the load-bearing capacity of the steel frame to prevent structural failure before the shotcrete installation; The safety factor of each calculation case is over 2.5, suggesting that the shotcrete thickness of 37 cm is overly conservative.

6.3 Influence of the Support Stiffness

The support stiffness significantly impacts the mechanical response of the structure throughout the entire construction process, and its

Table 5. Calculation Cases of the Support Stiffness

Shotcrete thickness d_{shot} /(cm)	Shotcrete stiffness k_{shot} /(MPa/m)	Ultimate bearing capacity /(MPa)	Allowable deformation/ (mm)
37	276	1.040	3.76
32	237	0.912	3.85
27	199	0.773	3.88
22	161	0.632	3.90

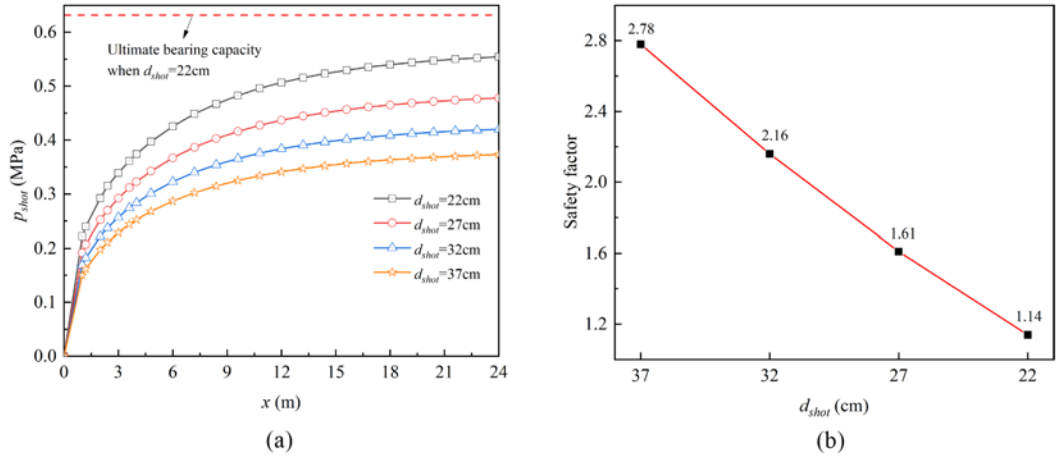

Fig. 14. Support Stress Development Curves and Safety Factors of the Shotcrete with Different Structural Stiffness: (a) Stress Development Curve, (b) Safety Factor

unreasonable allocation can lead to adverse application effects. If not allocated properly, the support stiffness may fail to satisfy the load-bearing requirements, or may result in a waste of resources. Herein, the support stiffness is regulated by adjusting the structural thickness, and the impact of support stiffness on the stress level and safety factor is analyzed. The calculation cases are listed in Table 5, presenting the structural stiffness, ultimate bearing capacity, and allowable deformation of the shotcrete based on Eqs. (11) – (13). Fig. 14 shows the stress development curves and safety factors of the shotcrete with different structural stiffness.

As depicted in Fig. 14(a), the stress of the shotcrete increases sharply within 3 m behind the tunnel face, then stabilizes as the distance from the tunnel face grows beyond 18 m; The final stress of the shotcrete progressively grows as its thickness decreases. When d_{shot} is 22 cm, the final stress nears the ultimate bearing capacity (0.632 MPa), registering at 0.556 MPa. As depicted in Fig. 14(b), the safety factor of the shotcrete declines notably with decreasing thickness. As d_{shot} decreases from 37 cm to 22 cm, the corresponding safety factors are 2.78, 2.16, 1.61, and 1.14, respectively, which highlights the impact of the shotcrete thickness on structural safety.

6.4 Sensitivity Analysis of Support Design Parameters on the Mechanical Response of Surrounding Rock and Supports

Sensitivity analysis is an essential approach for evaluating system stability by determining how changes in parameters affect the system's behavior, which is critical in assessing the impact of parameter disturbances on system characteristics (Zhou et al. 2020). The initial install locations and stiffness of the supports are the critical parameters affecting the effectiveness of tunnel support. Therefore, the system characteristics comprise surrounding rock deformation and support stress, and the influencing parameters consist of steel frame stiffness k_{set}, shotcrete stiffness k_{shot}, initial install location of the steel frame x_{ini}, and initial install location of the shotcrete x_1. Following the sensitivity analysis procedure used by Jiang et al. (2023), the sensitivity coefficients for various system characteristics can be derived, as listed in Table 6. The average sensitivity coefficients for surrounding rock deformation, steel frame stress, and shotcrete stress are utilized as the comprehensive assessment index for the supporting effect's sensitivity. This approach determines the sensitivity order of supporting effect to each design parameter as follows: Initial install location of shotcrete > Initial install location of steel frame > steel frame stiffness > shotcrete stiffness. Hence, the initial install location of each component of the support system should be taken as the crucial design parameter.

7. Comparison of the Effects of Different Support Methods

The staged support installation method entails creating an unbraced section and a low-stiffness support section behind the tunnel face, which can partially release the deformation of the surrounding rock to alleviate the pressure on the support system. To emphasize the benefits of the staged support installation method, this section compares the practical effects of the traditional support installation method with those of the proposed method. The two methods are presented as follows: the traditional method entails applying the steel frame and shotcrete simultaneously at the tunnel face, as shown in Fig. 15(a) and satisfies $x_{ini} = x_1 = 0$ m and $d_{shot} = 37$ cm, while the staged support installation method depicted in Fig. 15(b) involves creating an unbraced section and a low-stiffness support section behind the tunnel face, and satisfies $x_{ini} = 0.4$ m, $x_1 = 1.2$ m, and $d_{shot} = 27$ cm.

The surrounding rock deformation and support stress for each method are obtained by the proposed analytical solution. For the traditional method, the shotcrete stress is 0.374 MPa, the safety factor is 2.78, and the radial displacement of the inner wall is 67 mm.

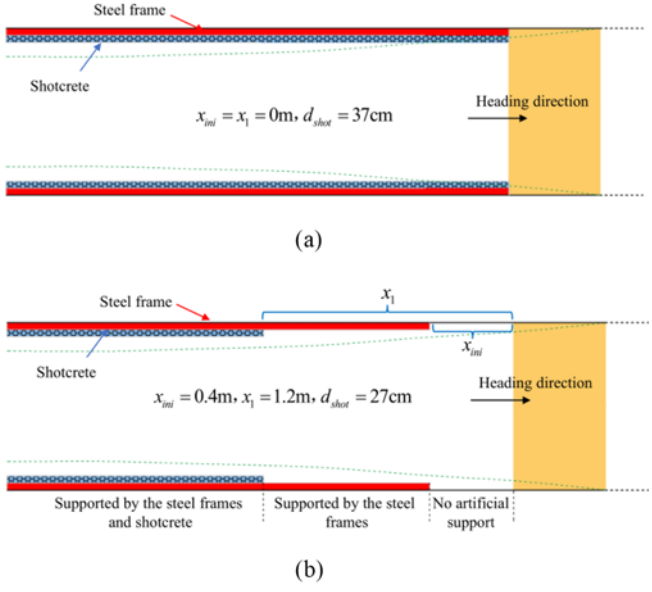

Fig. 15. Diagram of the Two Support Installation Methods: (a) Traditional Installation Method, (b) Staged Installation Method

Table 6. Sensitivity Coefficients for Various System Characteristics

Sensitive coefficient	Steel frame stiffness k_{set}	Shotcrete stiffness k_{shot}	Initial install location of steel frame x_{ini}	Initial install location of shotcrete x_1
Surrounding rock deformation	0.021	0.003	0.306	0.015
Steel frame stress	0.206	0.090	0.228	0.546
Shotcrete stress	0.265	0.129	0.174	0.541
Average	0.164	0.074	0.236	0.367

In contrast, for staged support installation, the shotcrete stress is 0.232 MPa, the safety factor is 3.33, and the radial displacement is 77 mm. It can be found that despite the shotcrete thickness of the second method being 10 cm less than that of the first method, the structural safety can be effectively guaranteed, and the deformation control effect does not degrade significantly. These results emphasize that the staged installation method can strike the perfect balance in terms of support bearing safety and deformation mitigating effects by adjusting the initial install location of each component. Moreover, this method can ease the load requirements for the support by utilizing the load-bearing capacity of the surrounding rock, reducing support thickness and thereby contributing to cost savings in engineering projects.

Based on the above analysis, it can be considered that the proposed model can be applied to obtain the mechanical response of the surrounding rock and artificial supports of the tunnel buried in red sandstone stratum when the support systems are installed in stages, which has the potential to overcome the limitations of stiff support systems in coping with large deformation problems of surrounding rock. In addition, the time-varying characteristics of surrounding rock and support are not considered in the theoretical derivation process, including the creep characteristics of surrounding rock (Wu et al., 2022b) and the hardening characteristics of shotcrete (Liu et al., 2023), which can be further improved in the subsequent research.

8. Conclusions

In this paper, the advantages of staged support installation method in enhancing the flexibility of the support system are analyzed. Combined with the elastoplastic analysis of surrounding rock in the red sandstone stratum, an analytical solution of interaction between surrounding rock and support is proposed. After verifying the rationality of the proposed solution, the influence of various parameters on the supporting effect is systematically investigated. The main conclusions are as follows:

1. The proposed analytical solution accounts for the intermediate principal stress, dilatancy and strain-softening characteristics of red sandstone, enabling a quantitative analysis of the interaction between surrounding rock and supports. This method offers a scientific guide for the staged installation of artificial supports, which has the potential to overcome the limitations of stiff support systems in coping with large deformation problems of surrounding rock.
2. When employing the staged installation method, the development trend of the steel frame stress shifts from rapid development to basic stability upon shotcrete installation. Postponing the initial install location of the steel frame can reduce its stress level and increase the stress level of shotcrete, whereas postponing the initial install location of shotcrete has an inverse effect. Excessive delays in support installation may cause the surrounding rock to enter the residual state and generate additional pressure, which is detrimental to structural safety.
3. The sensitivity order of supporting effect to each design parameter is as follows: Initial install location of shotcrete > Initial install location of steel frame > steel frame stiffness > shotcrete stiffness. The initial install location of each component of the support system should be taken as the crucial design parameter.
4. The staged installation method can achieve the optimal balance between structural safety and deformation control effects by adjusting the initial install location of the artificial support. This method can ease the load requirements for supports by utilizing the load-bearing capacity of the surrounding rock, and achieve cost savings in engineering by reducing support thickness.

Acknowledgments

This research was financially supported by the National Natural Science Foundation of China (No.51678498) and the High Speed Railway and Natural Science United Foundation of China (U1934213).

ORCID

Haiyan Xu https://orcid.org/0000-0003-3472-1036

References

Bernaud D, Quevedo FPM (2020) Analytical solution of deep tunnels in a strain-hardening elasto-plastic rock mass. *Latin American Journal of Solids and Structures* 17(6), DOI: 10.1590/1679-78256023

Chu ZF, Wu ZJ, Liu BG, Liu QS (2019) Coupled analytical solutions for deep-buried circular lined tunnels considering tunnel face advancement and soft rock rheology effects. *Tunnelling and Underground Space Technology* 94:103111, DOI: 10.1016/j.tust.2019.103111

Chu Z, Wu Z, Liu Q, Liu B, Sun J (2021) Analytical solution for lined circular tunnels in deep viscoelastic burgers rock considering the longitudinal discontinuous excavation and sequential installation of liners. *Journal of Engineering Mechanics* 147(4), DOI: 10.1061/(ASCE)EM.1943-7889.0001912

Deng CJ, Zheng YR, Wang K, Gao F (2009) Some discussion on the dilatancy of geotechnical materials. *Chinese Journal of Geotechnical Engineering* 27(3):283-287 (in Chinese)

Drescher A, Detournay E (1993) Limit load in translational failure mechanisms for associative and non-associative materials. *Geotechnique* 43(3):443-456, DOI: 10.1680/geot.1993.43.3.443

Duan SQ, Jiang XQ, Jiang Q, Xiong JC, Li CY (2023) Theoretical solution and failure analysis of water pressure on lining of deep-buried non-circular hydraulic tunnel based on the equivalent hydraulic radius method. *Engineering Failure Analysis* 148:107163, DOI: 10.1016/j.engfailanal.2023.107163

Guo W, Gao Y, Wu XZ, Liu SY, Fan PX (2022) Elastoplastic analysis of the enhancing mechanism of tensile performance of ductile thin-walled circular tubes with internal support. *Thin-Walled Structures* 171:108694, DOI: 10.1016/j.tws.2021.108694

Hu XR, Yu MH (2005) Amendment of the twin-shear criterion and its application to calculation of earth pressure. *Chinese Journal of Geotechnical Engineering* 27(3):283-287 (in Chinese)

Huang SB, He YB, Liu GF, Lu ZX, Xin ZK (2020) Effect of water content on the mechanical properties and deformation characteristics of the clay-bearing red sandstone. *Bulletin of Engineering Geology and the Environment* 80(2):1767-1790, DOI: 10.1007/s10064-020-01994-6

Jiang YF, Yu JY, Zhou P, Zhou FC, Lin JY, Li JY, Lin M, Lei FY, Wang ZJ (2023) Influence of traffic on the temperature field of tunnel in cold region: A case study on the world's longest highway spiral tunnel. *Underground Space* 8:196-209, DOI: 10.1016/j.undsp.2022.03.002

Li KS, Chen LX, Zhao Z, Liu CX (2023) Experimental investigation on mechanical, acoustic, and fracture behaviors and the energy evolution of sandstone containing non-penetrating horizontal fissures. *Theoretical and Applied Fracture Mechanics* 123, DOI: 10.1016/j.tafmec.2022.103703

Li WT, Li SC, Feng XD, Li SC, Yuan C (2011) Study of post-peak strain softening mechanical properties of rock based on Mohr-Coulomb criterion. *Chinese Journal of Rock Mechanics and Engineering* 30(7):1460-1466 (in Chinese)

Lin LB, Chen FQ, Lu YP, Li DY (2020) Complex variable solutions for tunnel excavation at great depth in visco-elastic geomaterial considering the three-dimensional effects of tunnel advance. *Applied Mathematical Modelling* 82:700-730, DOI: 10.1016/j.apm.2020.01.070

Liu C, Zhang DL, Zhang SL, Sun ZY (2023) Interaction analysis between composite supports and rheological rock considering progressive hardening characteristic of shotcrete. *Construction and Building Materials* 374:130876, DOI: 10.1016/j.conbuildmat.2023.130876

Luo Y (2018) Elastoplastic analysis on strain softening and fracture expansion of roadway surrounding rock based on D-P criterion. *Journal of Safety Science and Technology* 14(11):108-113, DOI: 10.11731/j.issn1673-193x.2018.11.017

Qiu JT, Shen YS, Zhang X, Zhang YF, Gan YH, Zhou XJ (2022) Simplified method for predicting time-dependent behavior of deep-buried tunnel considering tunnel excavation rate and stress release effects. *International Journal of Applied Mechanics* 14(5), DOI: 10.1142/S1758825122500430

Riabokon E, Poplygin V, Turbakov M, Kozhevnikov E, Kobiakov D, Guzev M, Wiercigroch M (2021) Nonlinear Young's modulus of new red sandstone: Experimental studies. *Acta Mechanica Solida Sinica* 34(6):989-999, DOI: 10.1007/s10338-021-00298-w

Sun ZY, Zhang DL, Fang Q, Dui GS, Tai QM, Sun FW (2021) Analysis of the interaction between tunnel support and surrounding rock considering pre-reinforcement. *Tunnelling and Underground Space Technology* 115:104074, DOI: 10.1016/j.tust.2021.104074

Vlachopoulos N, Diederichs MS (2009) Improved longitudinal displacement profiles for convergence confinement analysis of deep tunnels. *Rock Mechanics and Rock Engineering* 42(2):131-146, DOI: 10.1007/s00603-009-0176-4

Wang Q, Hu XL, Zheng WB, Li LX, Zhou C, Ying CY, Xu C (2021) Mechanical properties and permeability evolution of red sandstone subjected to hydro-mechanical coupling: Experiment and discrete element modelling. *Rock Mechanics and Rock Engineering* 54(5):2405-2423, DOI: 10.1007/s00603-021-02396-0

Wang ZJ, Xu JX, Xu JX, Zhou P, Xia Y, Li RY, Tang L (2018) Research on the deformation characteristics of tunnel surrounding rock in water-rich quaternary red sandstone stratum. *Journal of Railway Engineering Society* 35(9):54-60+109 (in Chinese)

Wen SY, Han LJ, Zong YJ, Meng QB, Zhang J (2013) Study on emission characteristics of sandstone uniaxial compression test with different moisture content. *Coal Science and Technology* 41(8):46-48+52, DOI: 10.13199/j.cnki.cst.2013.08.016 (in Chinese)

Wu K, Shao ZS, Qin S, Zhao NN, Chu ZF (2022b) An improved nonlinear creep model for rock applied to tunnel displacement prediction. *International Journal of Applied Mechanics* 13(8):2150094, DOI: 10.1142/S1758825121500940

Wu K, Shao ZS, Sharifzadeh M, Hong SY, Qin S (2022a) Analytical computation of support characteristic curve for circumferential yielding lining in tunnel design. *Journal of Rock Mechanics and Geotechnical Engineering* 14(1):144-152, DOI: 10.1016/j.jrmge.2021.06.016

Xu HY, Shao ZM, Wang ZJ, Cai LB, Li Z, Jiang XZ (2021) Sub-level classification and prediction system of fully weathered red sandstone rock mass based on physical property indices. *KSCE Journal of Civil Engineering* 25(3):1066-1085, DOI: 10.1007/s12205-021-0014-0

Yu MH (1994) Unified strength theory for geomaterials and its application. *Chinese Journal of Geotechnical Engineering* 16(2):1-10 (in Chinese)

Yu DM, Fan YF, Duan JX, Luo XW (2013) Elastoplastic unified solutions to deep-buried circular tunnels considering intermediate principal stress. *Journal of Shanghai Jiao Tong University* 47(9):1447-1453, DOI: 10.16183/j.cnki.jsjtu.2013.09.022 (in Chinese)

Zhang CG, Zhao JH, Zhang QH (2012) Convergence - confinement analysis of deep circular rock tunnels based on unified strength theory. *Chinese Journal of Geotechnical Engineering* 34(1):110-114 (in Chinese)

Zhao NN, Shao ZS, Chen XY, Yuan B, Wu K (2022) Prediction of mechanical response of "a flexible support system" supported tunnel in viscoelastic geomaterials. *Archives of Civil and Mechanical Engineering* 22(4), DOI: 10.1007/s43452-022-00485-7

Zhou H, Chen J, Lu JJ, Jiang Y, Meng FZ (2018) A new rock brittleness evaluation index based on the internal friction angle and class I stress-strain curve. *Rock Mechanics and Rock Engineering* 51(7):2309-2316, DOI: 10.1007/s00603-018-1487-0

Zhou SY, Guo XF, Zhang Q, Dias D, Pan QJ (2020) Influence of a weak layer on the tunnel face stability - Reliability and sensitivity analysis. *Computers and Geotechnics* 122, DOI: 10.1016/j.compgeo.2020.103507

Zhou P, Zhou FC, Lin JY, Li JY, Jiang YF, Yang B, Wang ZJ (2021) Decoupling analysis of interaction between tunnel surrounding rock and support in xigeda formation strata. *KSCE Journal of Civil Engineering* 25(12):4897-4912, DOI: 10.1007/s12205-021-0618-4